

Article

New Thermal Design Strategy to Achieve an 80-kg-Class Lightweight X-Band Active SAR Small Satellite S-STEP

Tae-Yong Park ¹, Bong-Geon Chae ¹, Hongrae Kim ¹, Kyung-Rae Koo ², Sung-Chan Song ² and Hyun-Ung Oh ^{3,*}

¹ Soletop Co., Ltd., 409 Expo-ro, Yuseong-gu, Daejeon 34051, Korea; typark@soletop.com (T.-Y.P.); bgchae@soletop.com (B.-G.C.); hrkim@soletop.com (H.K.)

² Satellite System Division, Hanwha System, 304 Cheoin-gu, Yongin City 449-886, Gyeonggi-do, Korea; kr.koo@hanwha.com (K.-R.K.); sungchan.song@hanwha.com (S.-C.S.)

³ Space Technology Synthesis Laboratory, Department of Smart Vehicle System Engineering, Chosun University (Agency for Defense Development: Additional Post), Pilmun-daero, Dong-gu, Gwangju 61452, Korea

* Correspondence: ohu129@chosun.ac.kr; Tel.: +82-62-230-7728; Fax: +82-62-230-7186

Abstract: The main objective of the S-STEP (the Small Synthetic Aperture Radar (SAR) Technology Experimental Project (S-STEP)) mission is developing an 80-kg-class active X-band SAR observation small satellite. For lighter, smaller, better, and cheaper development of the S-STEP system, a new thermal design strategy is essential. Therefore, we proposed a new thermal design strategy in this study. The main features of the proposed thermal design involve the minimization of heater power consumption by optimizing environmental heat fluxes on the satellite, the provision of long-term SAR imaging duration in both right- and left-looking modes, and the use of a lightweight flexible graphite sheet as a thermal interface for some high-power instruments. These features contribute to minimizing the satellite's mass budget through heater power minimization and achieving on-orbit system performance of S-STEP. The effectiveness of the proposed thermal design was numerically verified by on-orbit thermal analysis of the S-STEP system. In addition, the thermal design on a key payload component and the multifunctional transmit/receive module structure were verified through a space-simulated thermal vacuum test.

Keywords: thermal design; Synthetic Aperture Radar (SAR); small satellite; graphite sheet; thermal mathematical model



Citation: Park, T.-Y.; Chae, B.-G.; Kim, H.; Koo, K.-R.; Song, S.-C.; Oh, H.-U. New Thermal Design Strategy to Achieve an 80-kg-Class Lightweight X-Band Active SAR Small Satellite S-STEP. *Aerospace* **2021**, *8*, 278. <https://doi.org/10.3390/aerospace8100278>

Academic Editor: Paolo Tortora

Received: 25 July 2021

Accepted: 18 September 2021

Published: 24 September 2021

Publisher's Note: MDPI stays neutral with regard to jurisdictional claims in published maps and institutional affiliations.



Copyright: © 2021 by the authors. Licensee MDPI, Basel, Switzerland. This article is an open access article distributed under the terms and conditions of the Creative Commons Attribution (CC BY) license (<https://creativecommons.org/licenses/by/4.0/>).

1. Introduction

The so-called NewSpace paradigm refers to the recent commercialization of the space sector. The technology innovations of satellite and launch vehicles, as well as various relevant services, are now leading the rapid advances and growth of global space industries [1]. One of the technologies that plays an important role in the NewSpace era is the emergence of a small satellite constellation. The constellation of multiple satellites effectively reduces the system's temporal performances, such as revisit and response time, which enables frequent access to the target. The smaller, lighter, faster, better, and cheaper small satellite platform realized a large-scale constellation in orbit based on satellite mass production, which was nearly impossible with large-scale satellites [2]. The reduction of satellite launch cost, via reusable launch vehicles, small-scale launchers, and air-launch-to-orbit, have increased the satellite launch capability, thus contributing to the rapid orbital insertion of small satellites. These advantages make the small satellite platform attractive for implementing various low earth orbit (LEO) constellation missions, such as near real-time earth observation, global internet services, and communication networks, for commercial and military purposes [3–5].

The concept of a synthetic aperture radar (SAR), proposed in the 1960s, significantly changed the field of spaceborne remote sensing [6]. Its advantage compared with traditional

optical imaging is the ability to obtain high-quality images, even when the target area is in nighttime or covered with obstacles, such as cloud and fog. Owing to this imaging capability, the demand for SAR imagery in space has rapidly increased in various sectors, including government, military, and commercial sectors [7]. The constellation of small satellites with SAR instruments is a solution to meet the increasing demands. To date, many small SAR satellites, such as ICEYE X2, Capella X-SAR, StriX, and QPS-SAR, have been developed and launched by industries globally. They are in-orbital operations to provide SAR images at a 1 m class resolution [8–11]. To meet the various mission needs on spaceborne SAR imagery, the demand for an active phase array-type SAR antenna has been increasing for small satellite applications, as its electronic beam steering capability provides various SAR imaging modes, including stripmap, spotlight, and ScanSAR.

Proper thermal control is crucial to guarantee the functionality and thermo-mechanical stability of an SAR satellite with many high-power instruments in extreme on-orbit thermal environments. Traditionally, most SAR satellites have adopted flexible deployable SAR antenna panel structures [12] to achieve the desired SAR imaging performance. Thermal designs for SAR satellites have been mostly based on passive thermal control approaches using suitable thermal coatings, paints, thermal fillers, thermal insulators, radiators, multilayer insulation (MLI), and sun-shield. In addition, heat pipes and doublers have been applied to the radiator for effective heat dissipation of some high-power instruments, such as transmit/receive modules (TRMs) and electronics. The heat loss through the radiator was compensated by a heater. To date, several studies [13–15] have proposed and investigated the thermal design for SAR satellites based on thermal control hardware.

In addition to the small SAR satellites, Yang et al. [16] proposed a quasi-all-passive thermal control system (TCS) design for the Luojia 1-01 satellite with the problems of low thermal inertia and poor thermal conductivity of the satellite structure. They adopted surface coatings, thermal interface materials, MLI, and active heater control to achieve the minimum system mass and power budgets. Yendler et al. [17] proposed the thermal management system (TMS), which is capable of rejecting 1 kW of waste heat produced in the satellite. The TMS mainly consisted of rollout-type flexible deployable radiator, heat pipes integrated with the satellite structure, and phase change material with high heat storage capacity. They applied TMS to the 12U-class CubeSat and verified its effectiveness through the numerical thermal analysis. Ueno et al. [18] proposed functional thermal control systems for 100 W-class high-power 3U CubeSat. They used a heat storage panel with pitch type CFRP, micro loop heat pipe, and flexible re-deployable radiator. The effectiveness of adopting those thermal hardwares was numerically and experimentally verified. In all, a considerable number of previous studies reported thermal designs for small satellites [16–21].

For small SAR satellites, the light weight and compactness of onboard instruments are essential factors due to the limited mass and volume of satellite platforms. For a small satellite constellation mission, these factors would be far more essential because they are directly related to the available number of satellites launched at once. Currently, the adoption of the abovementioned passive thermal hardware might be the most suitable solution for the thermal control of small SAR satellites; however, the thermal design of small SAR satellites needs to be optimized for minimizing system mass and power budget allocated for a thermal control subsystem. In addition, it is necessary to minimize the heater's power consumption to achieve the compactness of the satellite by solar panel and battery size reduction.

An 80 kg class high-resolution earth observation small satellite with X-band active phase array SAR, named the Small SAR Technology Experimental Project (S-STEP) [22], is under development. For developing an S-STEP system in accordance with a smaller, lighter, faster, better, and cheaper NewSpace paradigm, several mechanical design strategies are being adopted for the satellite [22]. The design strategies involve a bus-payload integrated flat panel-type satellite platform, a multifunctional TRM structure, and a vibration-free orbital deployer (VFOD). The flat panel-type satellite structure does not require flexible

deployable structures, and it could be beneficial in terms of the dimensional stability of SAR antenna in extreme on-orbit thermal environments. The TRM assembly of S-STEP functions as a structural stiffener for the satellite structure and provides thermal dissipation through a radiator integrated with TRM. Thus, it can minimize the application of additional stiffener for the structural reinforcement of the satellite. These strategies make it possible to minimize the system mass budget while ensuring the structural safety of vibration-sensitive onboard instruments under launch loads. In particular, the structural design load reduction achieved by VFOD contributes to minimizing the development period and cost by optimizing the verification test process, i.e., streamlining and skipping the test phase or a step at a subsystem level can be positively considered. These advantages make it attractive to be used for implementing the NewSpace small SAR satellite. The effectiveness of these mechanical design strategies has been investigated by Kwon et al. [22]. However, this study did not perform the numerical or experimental verification of those thermal designs. To date, no other previous studies addressed the thermal design strategy for this form of small SAR satellite. In particular, no previous study qualitatively verified the thermal design to achieve the designated SAR imaging duration in both left- and right-looking modes of the small SAR satellite, although it is one of the most important system performance factors.

This study proposes a new thermal design strategy for assuring the functionality and thermal stability of the S-STEP system in an on-orbit thermal environment. The payload-bus integrated flat panel-type unique mechanical design of S-STEP requires efficient thermal control to achieve an SAR imaging duration of 60 s in both left- and right-looking modes and keep all onboard components within allowable temperature thresholds in orbit. For lighter, smaller, better, and cheaper development of the S-STEP system, the proposed thermal design strategy is based on the optimization of environmental heat fluxes acting on the satellite by passive thermal control using surface coatings, MLI, and radiators. In addition, a lightweight flexible graphite sheet with high thermal conductivity is used as conductive thermal paths between some high-power instruments and dedicated radiators. The multifunctional structure of TRM assembly provides effective thermal dissipation capability through the integrated radiators during SAR imaging. These strategies contribute to minimizing the satellite mass budget and heater power consumption, which help realize the implementation of a “lighter” SAR satellite. To verify the effectiveness of the proposed thermal design strategy, an on-orbit thermal analysis of the S-STEP system was performed. Further, the effectiveness of thermal design on the key payload components and multifunctional TRM structure was experimentally evaluated in a space-simulated thermal vacuum environment.

2. S-STEP System Overview

The S-STEP program has been started to develop an 80 kg class lightweight small SAR satellite for high-resolution SAR imagery for environmental investigation, surface mapping, and disaster monitoring. The mission operation concept of the S-STEP system is shown in Figure 1 [22]. The S-STEP system is operated at LEO and provides a 1 m resolution stripmap image, 4 m resolution ScanSAR image, and 1 m resolution VideoSAR for 10 s duration to capture the earth’s targets of interest. The SAR payload of S-STEP is an aperture-coupled cavity-backed microstrip patch array antenna, which can achieve high radio frequency (RF) gain. A total of 192 TRMs were applied to implement electronic beam steering capability in the elevation direction of the antenna. The SAR image data are transferred to an integrated avionics unit (IAU) for storage. The stored data are transmitted to the ground station through a 1 Gbps X-band downlink module. The expected mission lifetime of the S-STEP system is 3 years. The S-STEP program ultimately aims to implement a satellite constellation for near real-time SAR observation. Therefore, the S-band inter-satellite link (ISL) system is considered for immediate communication link between the satellites. Table 1 lists the basic system specifications of S-STEP [22].

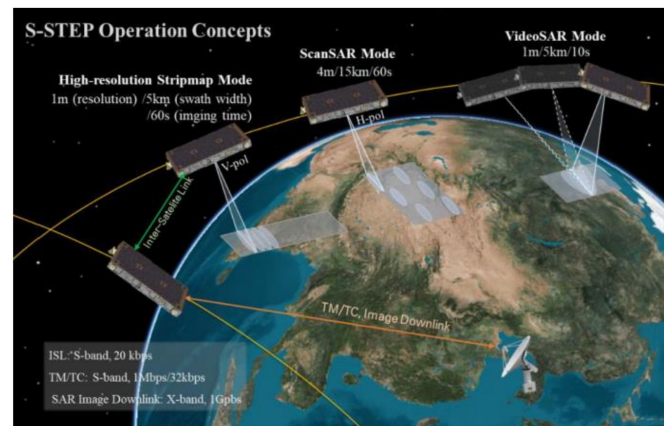


Figure 1. Mission operation concept for S-STEP system [22].

Table 1. System specifications for S-STEP [22].

Item	Specification
Mission lifetime	3 years
Satellite mass	80.3 kg
Satellite volume	1970 mm × 1060 mm × 200 mm
Power Generation	340 W (BoL)
Storage	648 Wh
Inter-satellite link	RF (S-band)
TM/TC/Image downlink	S-band/X-band
Attitude pointing accuracy	0.085° (3σ)
Resolution (@ SAR look angle: 25°)	- 1 m (Stripmap) - 4 m (ScanSAR) - 1 m (VideoSAR)
Swath (elevation × azimuth)	- 5 km × 420 km (Stripmap) - 15 km × 420 km (ScanSAR) - 5 km × 5 km (VideoSAR)
Image acquisition time (per single pass)	- 60 s (Stripmap) - 10 s (VideoSAR)

Figure 2 shows the mechanical configurations of the S-STEP satellite. The primary feature of its mechanical design is the bus–payload integrated flat panel-shaped satellite structure. This mechanical configuration is advantageous to ensuring the dimensional stability of the satellite, especially the SAR antenna, in extreme on-orbit thermal environments. One more essential feature of this satellite configuration is the additional 0 g compensation device for on-ground testing of SAR antennas, as it is a nondeployable-type antenna. All payload and bus electronic units are mounted on the top aluminum-skin honeycomb composite panel as the configuration shows in Figures 2c and 3. Four reaction wheels (RWs) in a pyramidal configuration with an optimal tilt angle are mounted at the center of the satellite to minimize the moment of inertia and their power consumption. The X-band antenna for payload data downlink and two S-band antennas for telecommand/telemetry (TM/TC) communication are installed on the side walls in $-x$, $+y$, and $-y$ sides of the satellite. The GPS and ISL antennas are also installed on various locations of the side walls. To operate the satellite, 340 W of electrical power is produced at beginning of life (BoL) and stores the power in the battery with 648 Wh capacity. Among the on-board instruments of satellite, the four TRM assemblies require the largest amount of power consumption. In the SAR imaging operation, the stored battery power is mainly used to operate these TRM assemblies.

The satellite is integrated on a VFOD introduced in a previous study [22], which has the dual functions of the orbital insertion of satellite and the entire spacecraft vibration isolation. The main function of VFOD is an on-orbit satellite separation combined with a side-mounting ride-share platform. The additional function of launch vibration isolation

was a key factor in minimizing the satellite mass, as the structural reinforcement was reduced by launch load mitigation. The multifunctional structure of payload components, the adoption of a new structural design methodology called Oh-Park methodology [23] for spaceborne electronics, and the proposed thermal design strategy contributed to further satellite mass reduction. The mass of the satellite was 80.3 kg due to these mechanical design strategies. A previous study [22] showed that the SAR performance index with respect to the satellite mass was close to those of the other small SAR satellites developed in accordance with the NewSpace paradigm. This study verified the feasibility of the proposed mechanical design strategies for S-STEP through satellite system-level structural analysis.

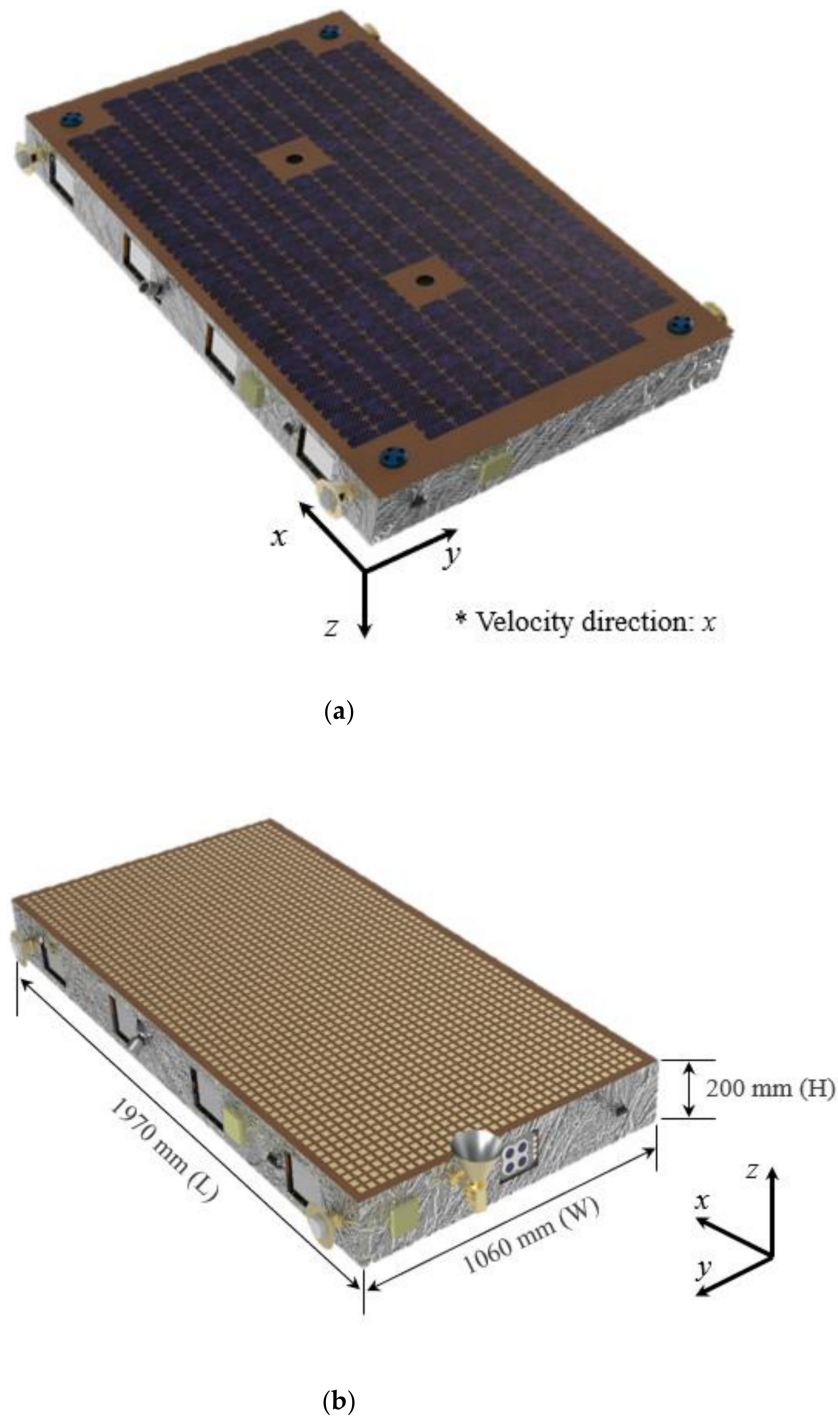
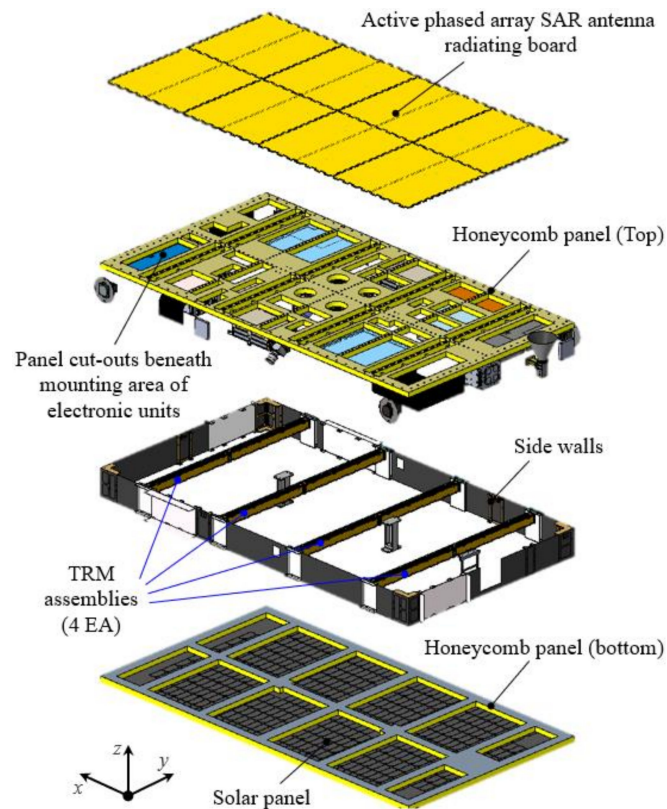


Figure 2. Cont.



(c)

Figure 2. Mechanical configurations of S-STEP satellite: (a) view from S/C $-z$ side, (b) view from S/C $+z$ side, and (c) exploded view.

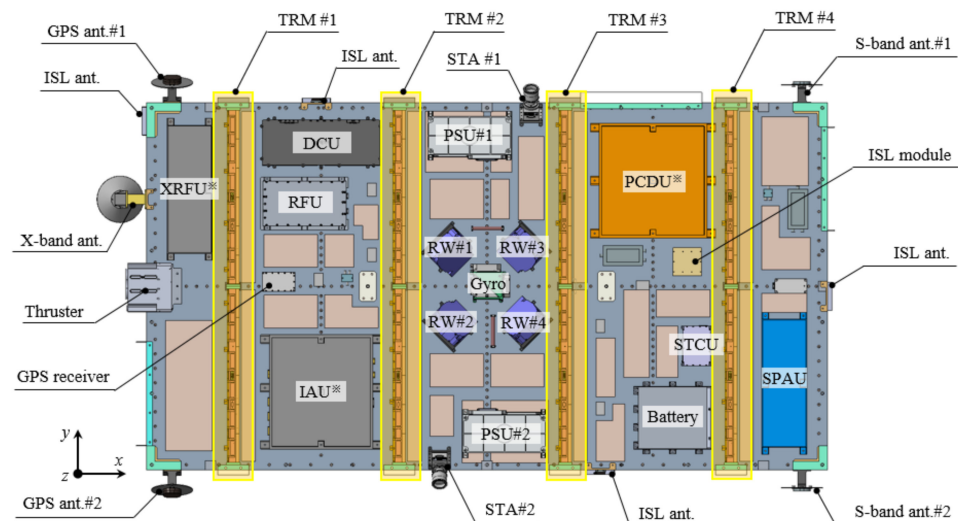


Figure 3. Internal configuration of S-STEP satellite (DCU: digital control unit; RFU: radio frequency unit; PSU: power supply unit; TRM: transmit/receive module; STA: star tracker assembly; RW: reaction wheel; ISL: inter-satellite link; IAU: integrated avionics unit; SPAU: S-band power amplifier unit; XRFU: X-band RF unit; PCDU: power conditioning and distribution unit; GPS: global positioning system; STCU: star tracker control unit).

3. New Thermal Design Strategy for S-STEP

The primary objective of establishing a new thermal design for S-STEP is to ensure long-term high-resolution SAR imaging duration for 60 s regardless of the right- and

left-looking modes of an SAR antenna. In addition, the thermal design shall maintain all onboard components within their allowable temperature limits (Table 2) in extreme on-orbit thermal environments with minimal use of heater power. To accomplish the thermal design objectives, the heat of the high-power components, such as the TRM assemblies, power conditioning and distribution unit (PCDU), IAU, and battery, shall be effectively dissipated to the outer space. These are the main focuses of the proposed thermal design. To implement a “lighter” satellite, the thermal design is mainly based on passive thermal control approaches using surface coatings, MLI, and heat dissipation radiators. The use of thermal hardware that occupy some portion of the mass to some extent, such as heat pipe and doubler used conventionally [13], are avoided for S-STEP.

Table 2. Allowable temperature limits of S-STEP components.

Component List		Allowable Temperature Limits [°C]				
		Operating		Non-Operating		
Category	Item	T _{min}	T _{max}	T _{min}	T _{max}	
Payload	TRM	#1	−20	60	−30	70
		#2	−20	60	−30	70
		#3	−20	60	−30	70
		#4	−20	60	−30	70
	DCU	−20	50	−30	60	
	RFU	−20	50	−30	60	
	PSU	#1	−20	50	−30	60
		#2	−20	50	−30	60
	SAR antenna (Radiating board)	−60	60	-	-	
C&DH	IAU	−20	50	−35	70	
EPS	PCDU	−20	50	−35	70	
	Battery	−30	60	-	-	
	Solar panel	−55	110	-	-	
CS	S-band ant.	#1	−40	80	−55	85
		#2	−40	80	−55	85
	SPAU	−20	50	−35	70	
	X-band ant.	−40	70	−55	85	
	XRFU	−20	50	−35	70	
	ISL ant.	#1	−40	85	-	-
		#2	−40	85	-	-
		#3	−40	85	-	-
#4		−40	85	-	-	
ISL module	−25	65	-	-		
Bus	Gyro	#1	−40	65	−55	85
		#2	−40	65	−55	85
		#3	−40	65	−55	85
	STA	#1	−20	40	−30	70
		#2	−20	40	−30	70
	STCU	−20	50	−30	70	
	GPS Receiver	−20	60	−40	85	
	GPS ant.	#1	−25	55	−30	60
		#2	−25	55	−30	60
	MAG	−25	70	-	-	
	CSS (Coarse Sun Sensor)	#1	−25	70	-	-
		#2	−25	70	-	-
		#3	−25	70	-	-
		#4	−25	70	-	-
	RW	#1	−20	60	−30	70
#2		−20	60	−30	70	
#3		−20	60	−30	70	
#4		−20	60	−30	70	
Propulsion	Thruster	−20	40	−40	65	

Figure 4 shows the new thermal design concept for the proposed S-STEP system. The front SAR antenna surface ($-z$ side) and side walls (x and y sides) are exposed to relatively lower environmental fluxes. Therefore, these surfaces can be used for dissipating satellite internal heat to outer space. Moreover, the incoming solar heat flux on the solar panel ($+z$ side) can be used as a heat source to compensate for heat loss. The optimization of solar heat flux and heat dissipation of the satellite is achieved by applying various thermal coatings, MLIs, and radiators to control the heat exchange between structural elements and components, which results in minimizing the heater power budget, contributing to further satellite mass reduction due to decreases in solar panel and battery sizes. This thermal design concept is the most innovative and unique aspect of the proposed thermal design strategy for S-STEP that has never been attempted in the previous small SAR satellite programs.

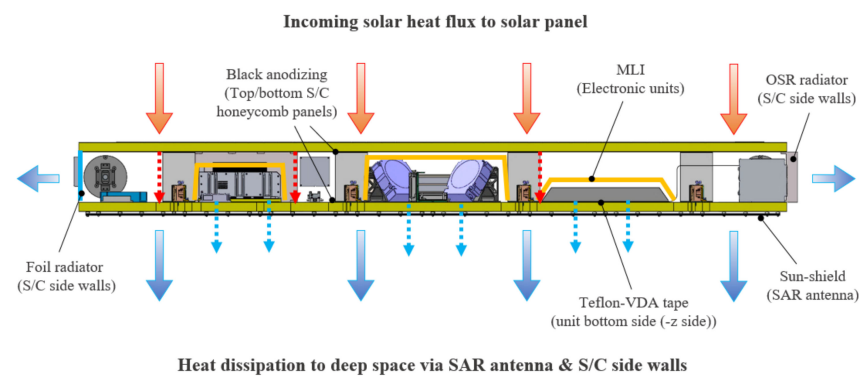


Figure 4. The proposed thermal design concept for S-STEP satellite.

In the thermal design, an RF-transparent sunshield covers the external side of the SAR antenna for heat rejection. The primary satellite structures of aluminum-skin honeycomb panels are black anodized for minimizing the thermal gradient over the entire satellite structure by facilitating the internal heat exchange. The internal waste heats of payload and bus electronic units and solar panels are dissipated via mounting surfaces ($-z$ side) to the SAR antenna. Thus, most honeycomb panel areas, including the mounting areas for electronic units, were cut-out for their effective heat dissipation (Figure 2c). These cut-outs were advantageous to reduce the satellite mass as well. The electronic unit mounting surfaces ($+z$ side) were coated with Teflon-VDA tape with high emissivity. The rest of their surfaces were covered with MLI to avoid the absorption of heat radiated from the solar panel. For further heat dissipation, second surface mirror (SSM) foil radiators were integrated on the sidewalls (Figure 5).

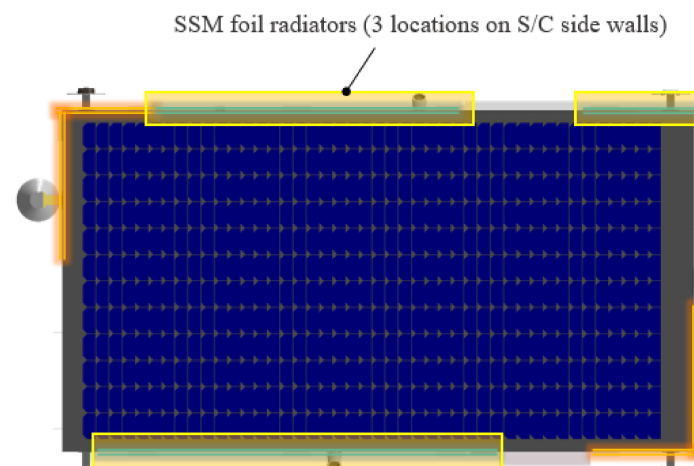
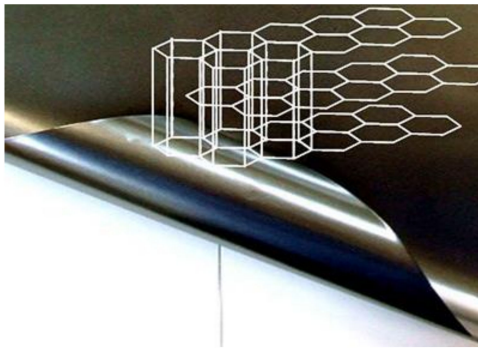


Figure 5. Allocation of SSM foil radiators on S-STEP satellite.

For effective heat dissipation of PCDU, IAU, and battery producing relatively larger amount of waste heat than the others, this study focused on the unique characteristics of a lightweight flexible graphite sheet. The graphite sheet is a popular thermal interface material and has been used in various fields, such as portable devices, electronics, and space engineering [24]. It has many advantages, such as high thermal conductivity in the in-plane direction of the sheet (four times higher than copper), light weight, flexibility to bending, high heat-resistance, and availability to use in a vacuum. All these characteristics make the graphite sheet attractive to use for thermal control of small satellites with a limited mass budget. Table 3 lists the specifications of the graphite sheet used for the S-STEP satellite. In the S-STEP thermal design, the graphite sheet was used to form the heat transfer paths from the IAU, PCDU, and battery to the dedicated radiators, respectively (Figures 6 and 7a). Both ends of the graphite sheet were clamped on the unit and radiator, respectively, to implement a secure thermal contact. For PCDU, where a larger amount of heat rejection is required than others, two radiator assemblies with graphite sheets were applied to the unit. The thermal control solution using a graphite sheet could be more advantageous than the conventional heat pipe in terms of light weight and unnecessary to maintain the orientation to the horizontal plane of the pipe to avoid the gravitational effect during an on-ground test. A total of 15 graphite sheet layers, determined on the basis of a previous study [25], were applied with respect to each component.

Table 3. Specifications of lightweight flexible graphite sheet [24].

Item	Specification
Manufacturer	KANEKA Co.
Configuration	
Thickness	40 μm
Conductivity	- 1500 W/m/K (In-plane) - 5 W/m/K (Out-of-plane)
Density	2 g/cm ³
Flexibility	- Minimum curvature radius = 2 mm, 180° angle - Withstands repeated bending more than 10,000 times - Ease of manufacturing such as punching and bending
Features	- High electromagnetic shielding effect - Extremely low water absorption - Availability to use in vacuum environment

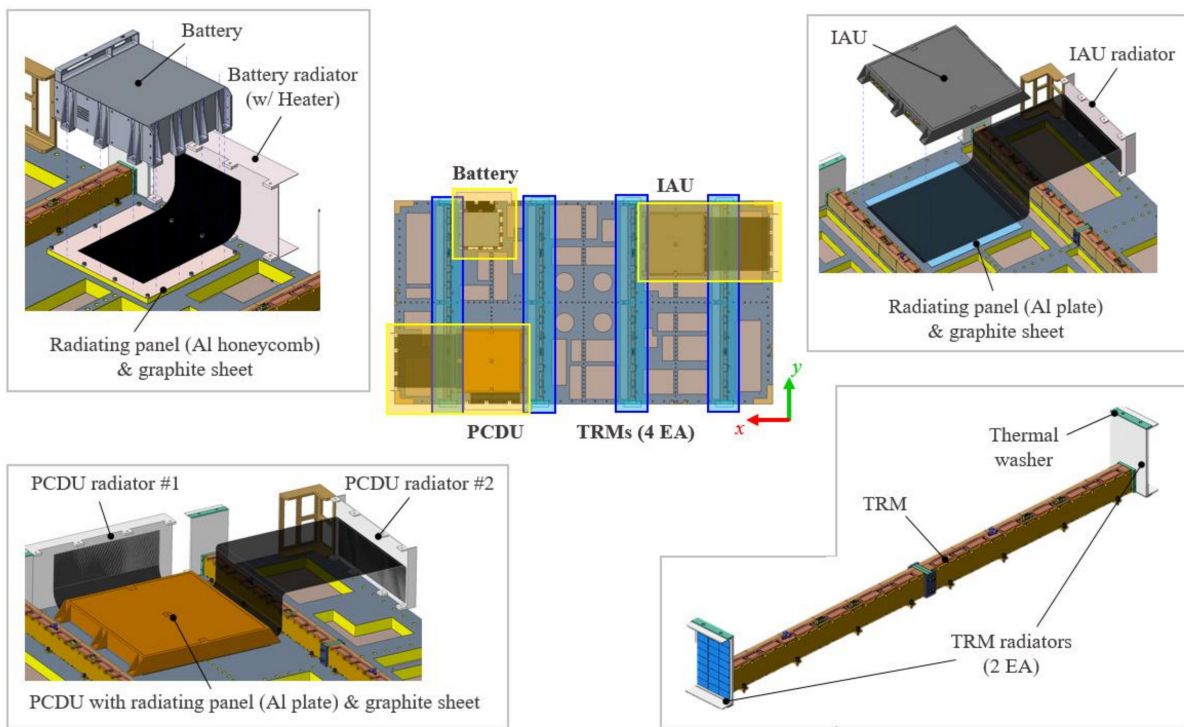


Figure 6. Thermal design concept for high-power components.

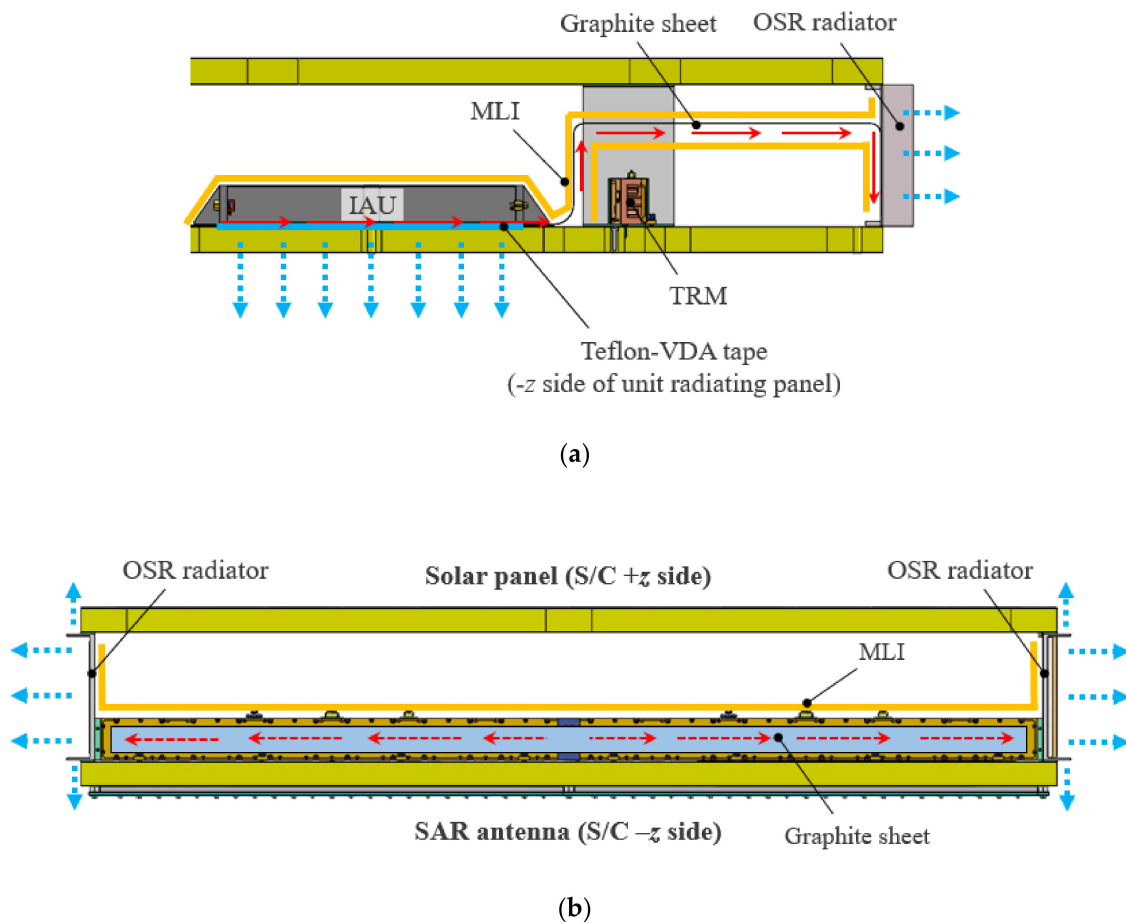


Figure 7. Examples of thermal paths for heat dissipation of high-power components: (a) IAU and (b) TRM.

In the thermal design, the battery module is the only component requiring heater control for temperature management to maintain the electrical power storage capacity. This fact indicates that the power budget-saving can be expected based on the proposed thermal design strategy. A Kapton polyimide film heater was attached adjacent to the battery radiator. Through the preliminary thermal analysis, the on/off set-points of the heater are set as 15/16 °C, and the heater power was determined as 30 W to satisfy the requirement of heater duty to be lower than 80%.

The effective heat dissipation of TRM is a crucial factor in achieving the long-term SAR imaging duration of 60 s in both left- and right-looking modes of SAR antenna in orbit. In the previous study [22], the concept of the multifunctional TRM assembly structure was introduced as the configuration shown in Figure 6. A single TRM assembly was integrated with two optical solar reflector (OSR) radiators at both ends to effectively dissipate the heat produced during SAR imaging operation (Figure 7b). In this study, the U-shaped configuration of each radiator further enhanced the heat dissipation capability by increasing the radiating area. In addition, the proposed design was intended to dissipate heat to the bent parts of the radiator, even if the incidence angle of heat flux varied with the attitude maneuvering of the satellite. The radiator design also provided mechanical interfaces to integrate the top and bottom honeycomb panels of the satellite. To minimize the thermal gradient over the TRM assembly, a graphite sheet was integrated along its sidereal surface. The TRM assembly was radiatively and conductively decoupled from the satellite using MLI and thermal washers to secure heat dissipation capability.

4. On-Orbit Thermal Analysis of S-STEP

4.1. Overview of Thermal Analysis

To verify the effectiveness of the proposed thermal design strategy in meeting the design objectives of the S-STEP system described in Section 3, a system-level transient on-orbit thermal analysis was performed. Table 4 lists the orbital conditions used for the thermal analysis. The hot and cold conditions are defined in the table to implement critical thermal environments on the satellite. The hot and cold cases corresponded to when the satellite was exposed to the highest and lowest environmental heat fluxes, respectively. The thermal analysis cases are defined in Table 5. Cases 1 and 2, respectively, correspond to the SAR imaging operation in the left- and right-looking modes for the hot environment. Cases 3 and 4, respectively, correspond to the SAR imaging operation in the left- and right-looking modes for the cold environment. Case 5 corresponds to the safe-hold mode for the cold environment.

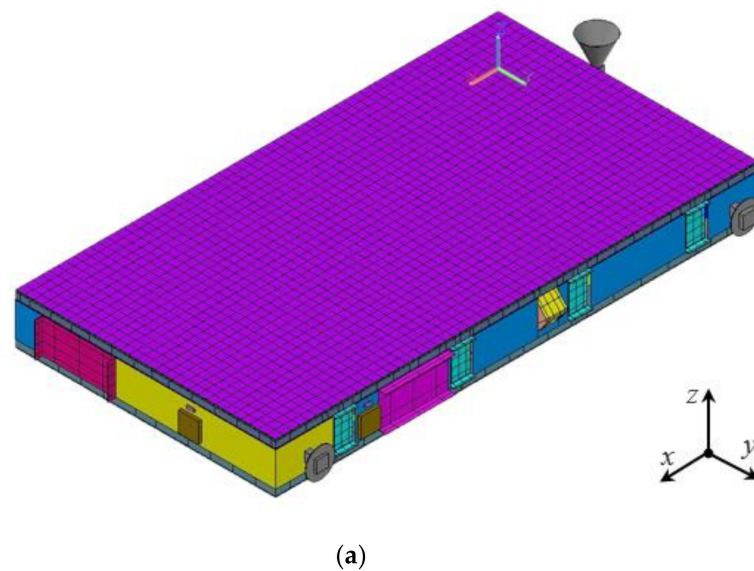
Table 4. Orbital conditions used for on-orbit thermal analysis.

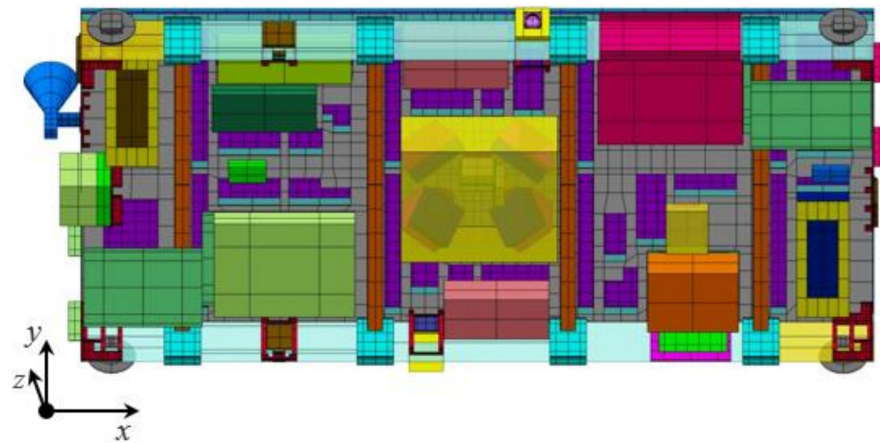
Item	Cold Case	Hot Case
Altitude (km)	523.87	524.96
RAAN (deg)	352.34	186.03
Eccentricity	0.00075515	0.00075515
Orbit inclination (deg)	44.2	44.2
Date (yyyy.mm.dd hh:mm:ss)	2024.03.08 07:19:07	2025.12.25 00:25:12
Beta angle (deg)	−0.94	−67.49
Solar constant (W/m ²)	1287	1420
Albedo	0.30	0.35
Planetary flux (W/m ²)	227	249

Table 5. On-orbit thermal analysis case definition.

Analysis Case	Environmental Condition	Operation Phase	Attitude	SAR Payload Operation	G/S Contact
1	Hot case	SAR imaging	Left-looking	Operation	O
2	Hot case	SAR imaging	Right-looking	Operation	O
3	Cold case	SAR imaging	Left-looking	Operation	O
4	Cold case	SAR imaging	Right-looking	Operation	O
5	Cold case	Safe-hold	Sun pointing	Non-operation	X

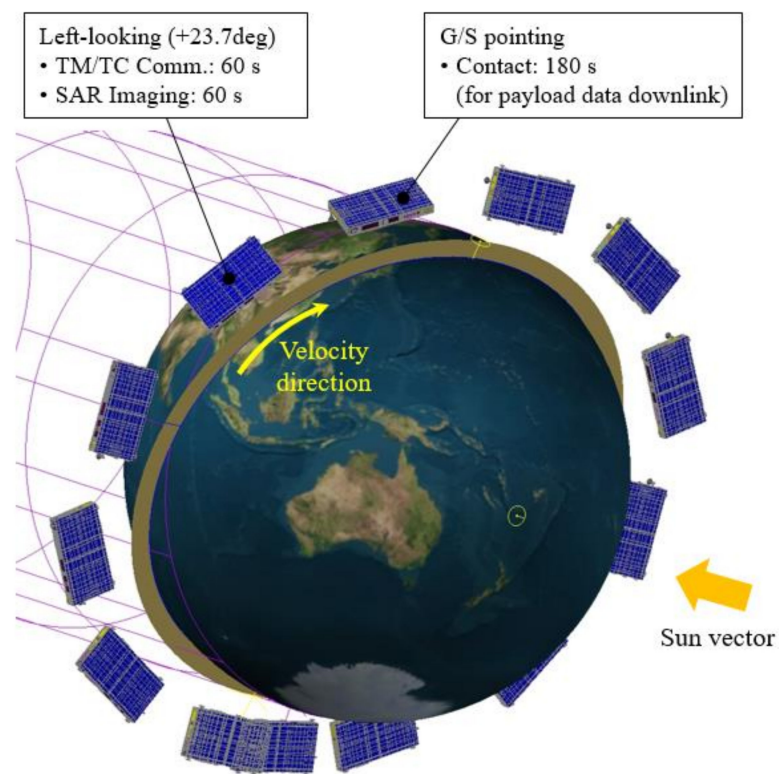
Figure 8a,b, respectively, show the external and internal configurations of a thermal mathematical model (TMM) of the S-STEP system for on-orbit thermal analysis. A total of 13,718 nodes were used for modeling the TMM. The TMM was constructed using Thermal Desktop [26], a CAD-based geometric interface of the commercial on-orbit thermal analysis tool of Systems Improved Numerical Differencing Analyzer/Fluid Integrator (SINDA/FLUINT) [27]. A RadCAD was used to calculate the radiation exchange factors and orbital heating rates based on the geometrical mathematical model (GMM) created by Thermal Desktop. The GMM and output data of RadCAD were used as inputs for on-orbit thermal analysis using SINDA/FLUINT. The representative orbital profiles of S-STEP created based on the information specified in Table 4 are shown in Figure 9a–c. In the SAR imaging operation, the satellite sequentially performed TM/TC communication (60 s), SAR imaging (60 s), and ground station (G/S) pointing for image data downlink (180 s). In the safe-hold mode, the satellite maintained the Sun-pointing of the solar panel (Figure 9c). Tables 6 and 7, respectively, list the thermo-physical and -optical properties used for the thermal analysis. The thermal network was implemented using a node-to-node conductor or a surface-to-surface contactor in the thermal desktop.

**Figure 8.** Cont.



(b)

Figure 8. Thermal mathematical model (TMM) of S-STEP satellite: (a) view from +z side and (b) internal configuration.



(a)

Figure 9. Cont.

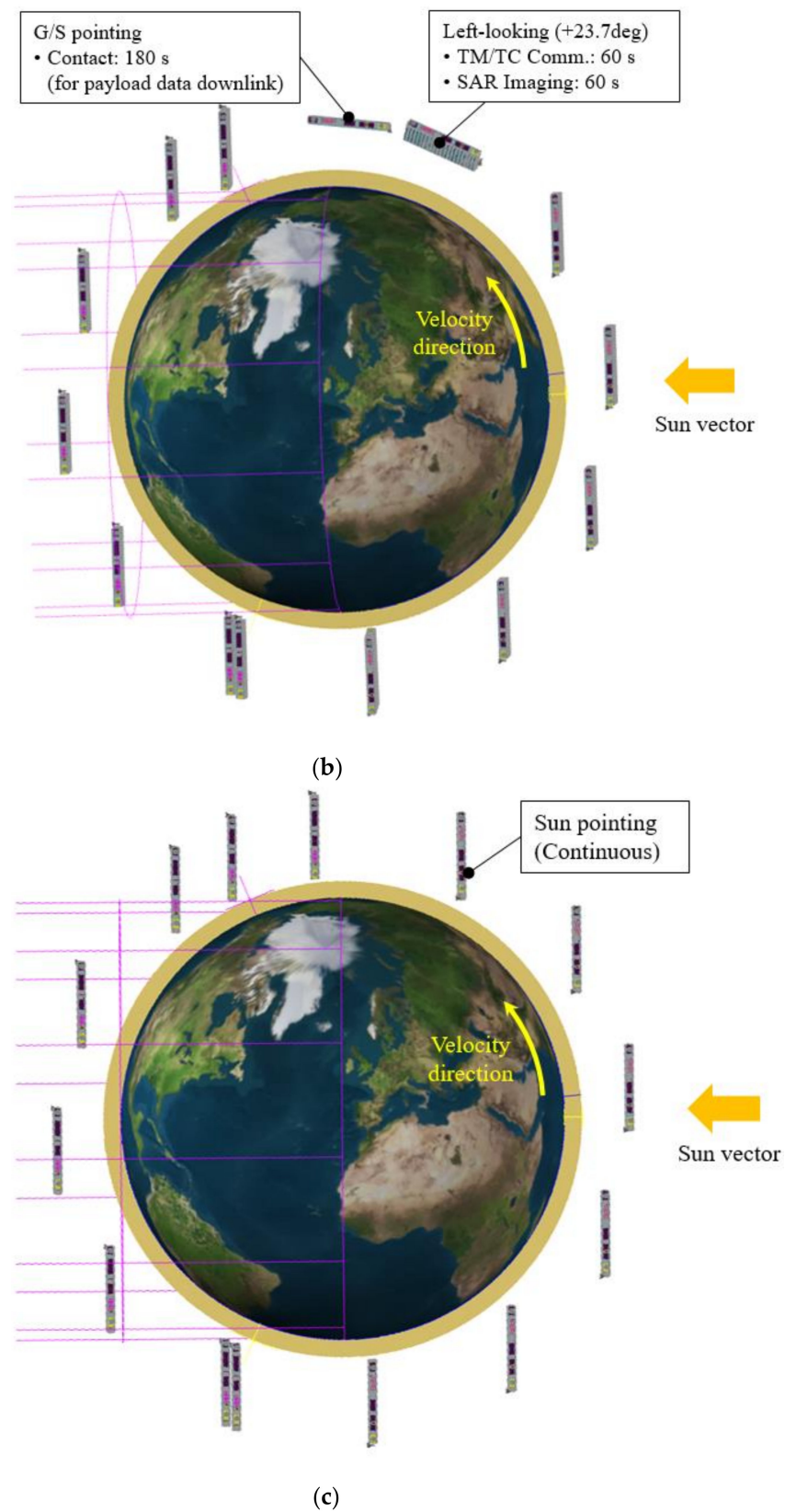


Figure 9. Representative orbital temperature profiles of S-STEP in left-looking SAR imaging operation: (a) hot environment, (b) cold environment, and (c) safe-hold mode.

Table 6. Thermo-physical properties used for thermal analysis.

Material	Conductivity (W/m/K)	Density (kg/m ³)	Specific Heat (J/kg/K)	Remark
Al-6061	170	2768	879.2	Unit, radiator, brackets
Al-7075	121.2	2770	961.2	Honeycomb panel (Facesheet)
CFRP	30	1910	711.76	Solar panel
Graphite sheet	$k_X = 1200$ $k_Y = 1200$ $k_Z = 5$	1200	1200	Graphite sheet, 15 layers stacked [25]
Honeycomb core	$k_X = 3.25$ $k_Y = 2.17$ $k_Z = 7.71$	129.75	921.6	Honeycomb panel (Core)
Foil radiator	0	300	1200	Foil radiator
Kevlar honeycomb	0.40	96	1420	SAR antenna radiating board
RF-35A2	0.29	2280	990	SAR antenna radiating board
Sun shield	1000	206	1200	Sun shield
MLI	0	300	1200	MLI

Table 7. Thermo-optical properties used for thermal analysis.

Material	Absorptivity [α]	Emissivity [ϵ]	α/ϵ	Remark
Alodine	0.35	0.07	5.00	Radiator, structural brackets
Black anodizing	0.88	0.88	1.00	Honeycomb facesheet, battery mounting I/F plate, foil radiator (Inside)
Kapton	0.35	0.40	0.88	Honeycomb core (Edge)
Gold coating	0.23	0.05	4.60	TRM (SAR ant. side)
Graphite sheet	0.66	0.30	2.20	Graphite sheet
MLI	0.05	0.05	1.00	MLI, electronic units
OSR	0.11 (BOL) 0.24 (EOL)	0.80	0.14 (BOL) 0.30 (EOL)	Radiator
PTFE	0.12	0.85	0.14	SAR antenna (+z-axis)
Solar cell	0.61	0.83	0.90	Solar panel
Sun shield	0.46	0.14	3.29	Sun shield (Inside)
Sun shield	0.43 (BOL) /0.56 (EOL)	0.69	0.62 (BOL) 0.81 (EOL)	Sun shield (Outside)
Teflon tape	0.11 (BOL) /0.25 (EOL)	0.72	0.15 (BOL) 0.35 (EOL)	Foil radiator, bottom side of electronic units (+z-axis), solar panel
Antenna	0.25	0.75	0.33	GPS ant., ISL ant., S-band ant.
VDA	0.065	0.023	2.83	GPS ant., ISL ant., S-band ant.
Al-VDA	0.09	0.028	3.214	Honeycomb panel (Local)

4.2. Results of Thermal Analysis

Figure 10 shows the representative thermal analysis results for Case 1—the orbital temperature profiles of components newly developed in this program when the left-looking SAR imaging operation was executed in the hot environment. This is the worst hot condition for the S-STEP system among the analysis cases listed in Table 5. Temporal temperature variations occurred due to the changes in incidence angle of satellite with respect to the sun and earth in accordance with the orbital revolution of satellite, as shown in Figure 9. The thermal design to dissipate the heat of electronic units through SAR antenna controlled their temperatures well, especially high-power electronic units, such as PCDU, IAU, and battery, combined with sidewall radiators and thermal paths implemented by the graphite sheet. The key payload components of TRM assemblies were operated under a moderate temperature condition, ranging from 29.6 to 42.2 °C, despite their total heat dissipation of 1460 W (365 W per a single TRM assembly) during SAR imaging operation. Figure 11a,b, respectively, show the predicted maximum and minimum temperatures of all onboard components in Case 1 (left-looking) and Case 2 (right-looking) when the SAR imaging operation is executed in the hot environment. The graph also shows the operating and survival temperature limits of each component. In both cases, the temperatures of all components were maintained within their allowable limits for the operating conditions specified in Table 2. In particular, the high-power components of IAU and PCDU were operated with sufficient temperature margins of more than 6.7 °C by effective heat dissipation via the SAR antenna and sidewall radiators. The battery temperature was maintained above 25.3 °C, and the heater was not operated during the entire orbit. These analysis results indicated that the proposed thermal design strategies were effective for stable satellite operation and achieving the required SAR imaging duration of 60 s, regardless of SAR left- and right-looking modes, even in the worst hot environment.

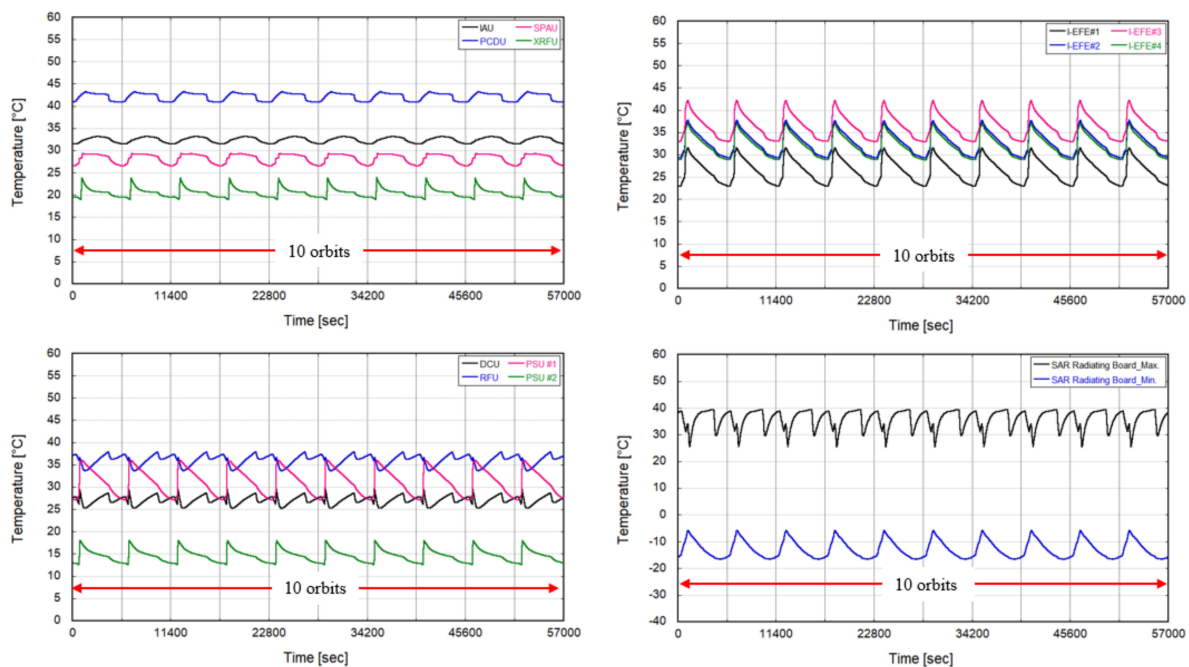
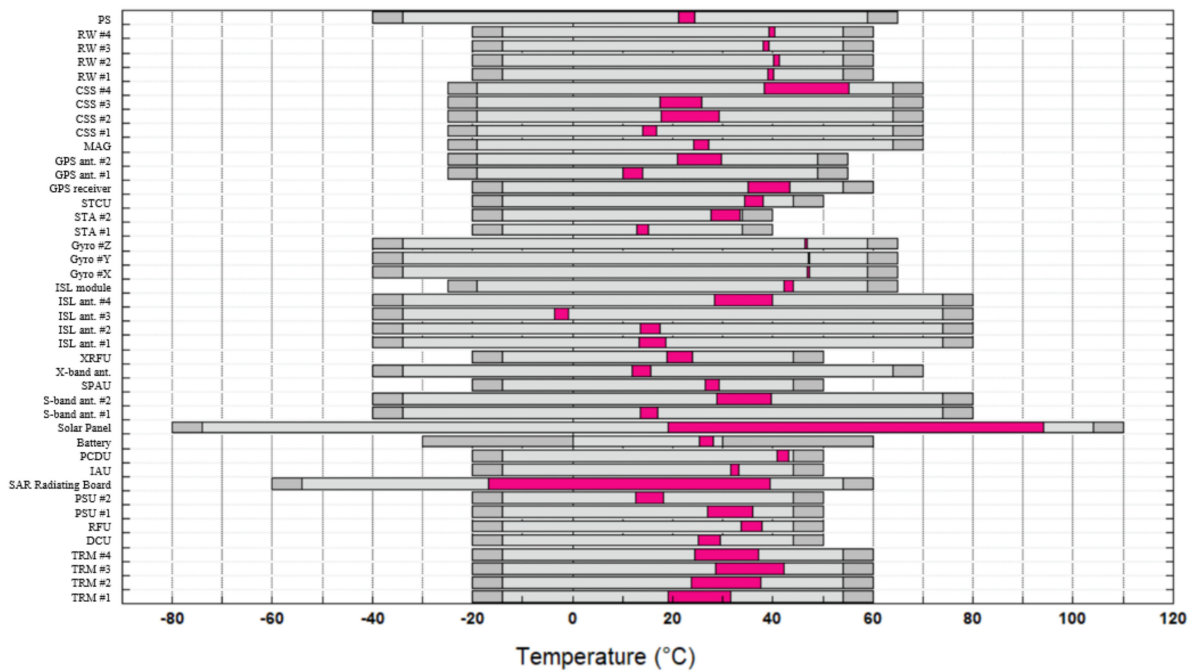
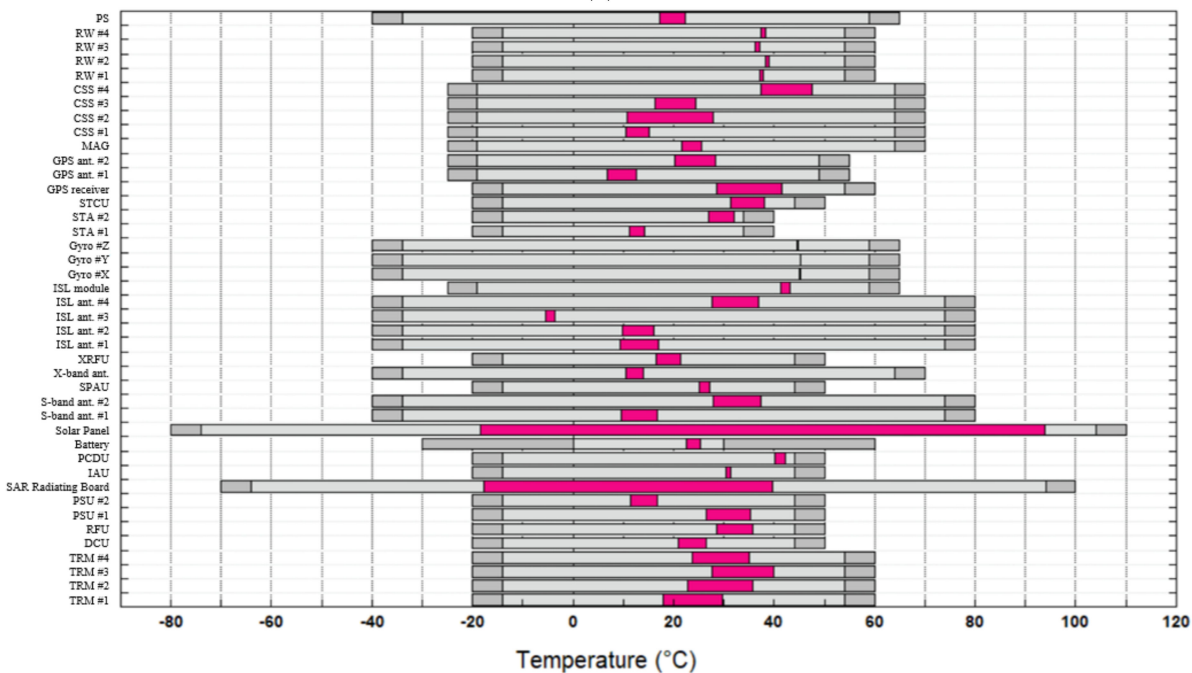


Figure 10. Predicted on-orbit temperature profiles of components newly developed in S-STEP program (Cases 1) (SAR left-looking mode in hot environment).



(a)



(b)

Figure 11. Predicted maximum and minimum temperatures of S-STEP components in hot environment (Cases 1 and 2): (a) SAR left-looking mode and (b) SAR right-looking mode.

Figure 12 shows Case 3 analysis results—the orbital temperature profiles of representative onboard components when left-looking SAR imaging operation is executed in the cold environment. The predicted maximum and minimum temperatures of the entire onboard components in Case 3 (left-looking) and Case 4 (right-looking) when the SAR imaging operation was executed in the cold environment are shown in Figure 13a,b, respectively. These figures show that all components were within the temperature ranges of operating conditions. The temperatures of TRMs were moderately maintained within the range of -5.6 to 0 °C in both the left- and right-looking modes of SAR antenna. The

battery temperature was maintained above 14 °C by heater control, and the duty was 36%. Figure 14 shows the thermal analysis results in Case 5 (safe-hold mode, cold environment). All non-operating components kept the temperature within the survival limits. The heater duty was 39% in this case. These on-orbit thermal analysis results showed that the proposed S-STEP system would be stably operated throughout the mission duration under the expected on-orbit thermal environment.

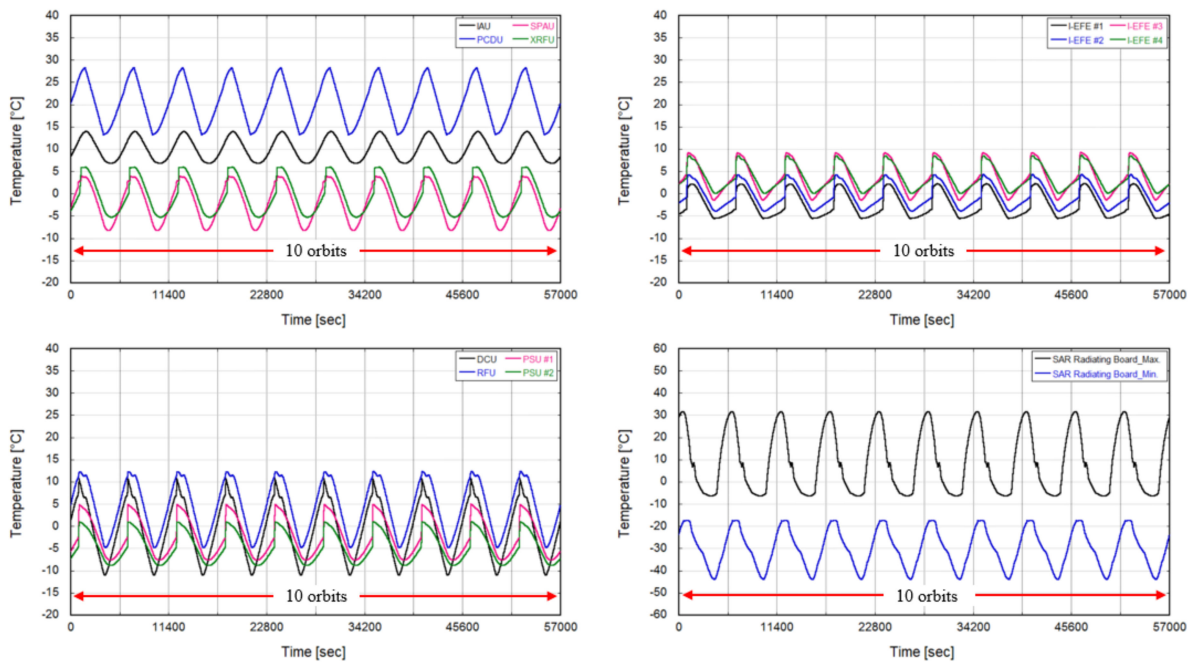
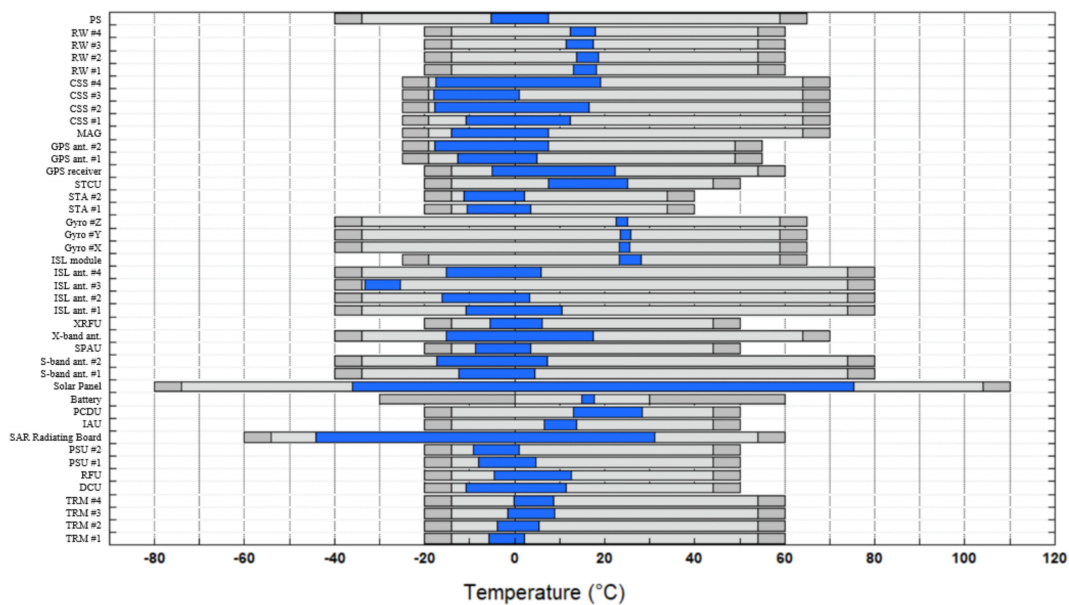
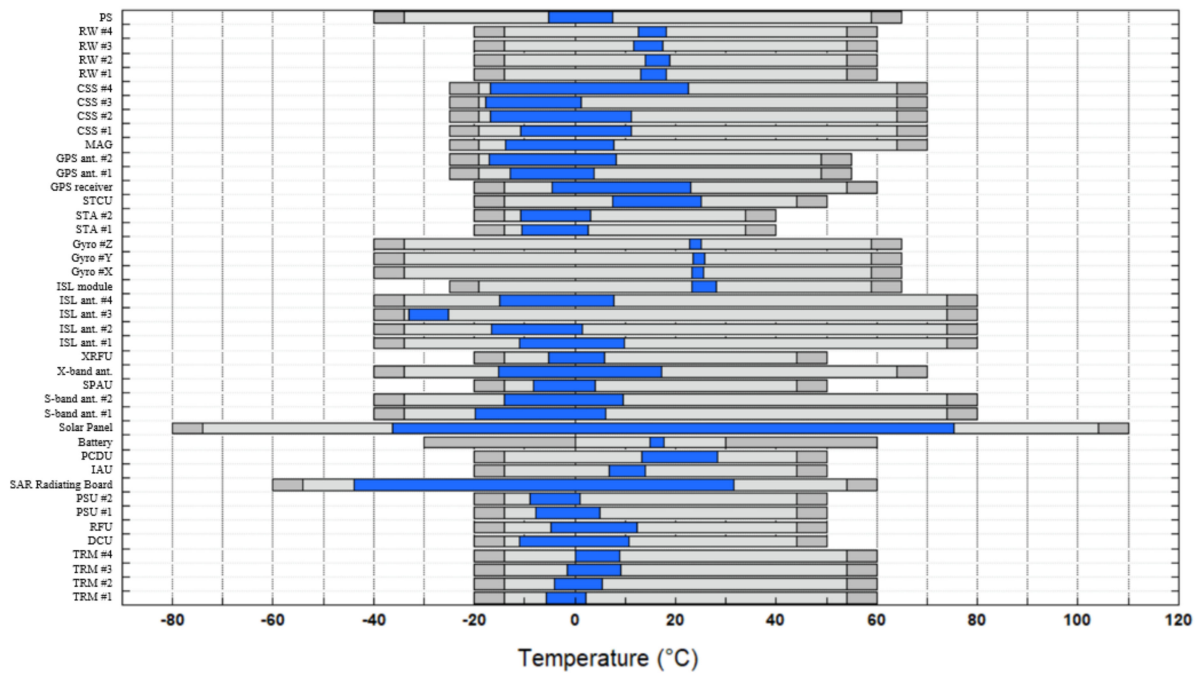


Figure 12. Predicted on-orbit temperature profiles of components newly developed in S-STEP program (Cases 4) (SAR right-looking mode in cold environment).



(a)

Figure 13. Cont.



(b)

Figure 13. Predicted maximum and minimum temperatures of S-STEP components in cold environment (Cases 3 and 4): (a) SAR left-looking mode and (b) SAR right-looking mode.

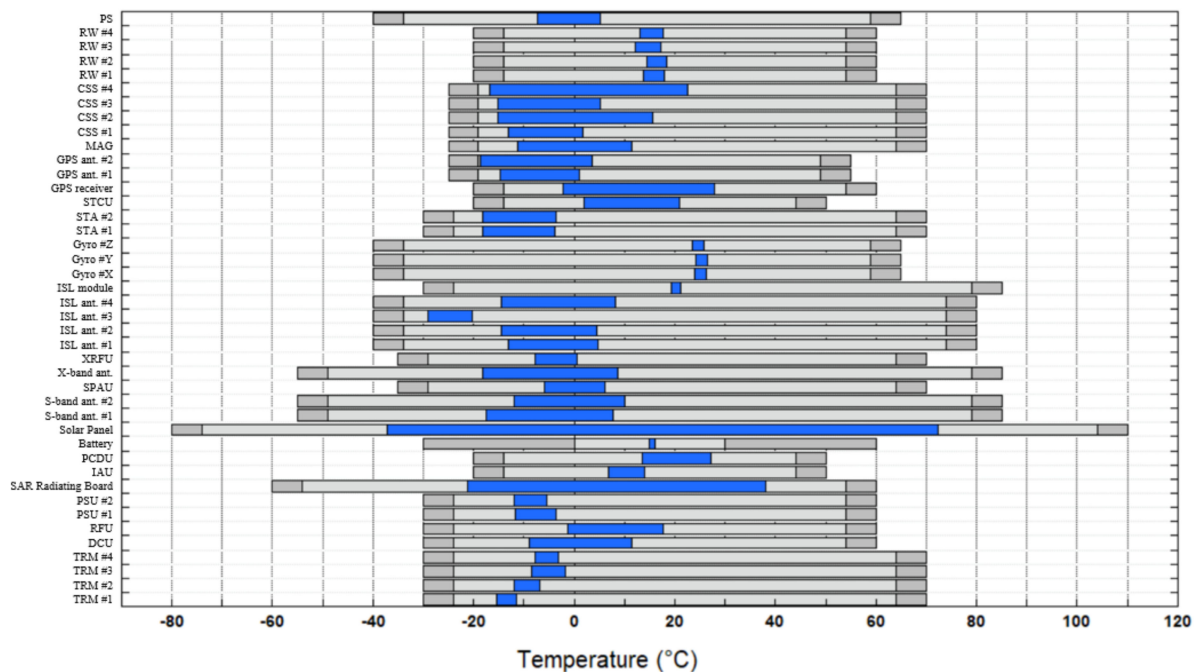


Figure 14. Predicted maximum and minimum temperatures of S-STEP components in safe-hold mode in cold environment (Case 5).

The TRM exhibits temperature-dependent RF output characteristics, such as gain and phase errors, which negatively affect in-antenna beam formation [28]. Although the S-STEP SAR payload has an output error compensation function, an additional technique to contribute to the error compensation, in the thermal control perspective, might be to reduce the spatial temperature difference (ΔT_s) over the TRM assemblies. Figure 15 shows the analyzed temperature contour of four TRM assemblies at the time when the maximum

ΔT_s occurred during the left-looking SAR imaging in the hot case. Table 8 summarizes ΔT_s of each TRM in the left- and right-looking modes in the hot and cold environments (Cases 1–4). The ΔT_s values of TRMs did not increase more than 7.6 °C in all cases.

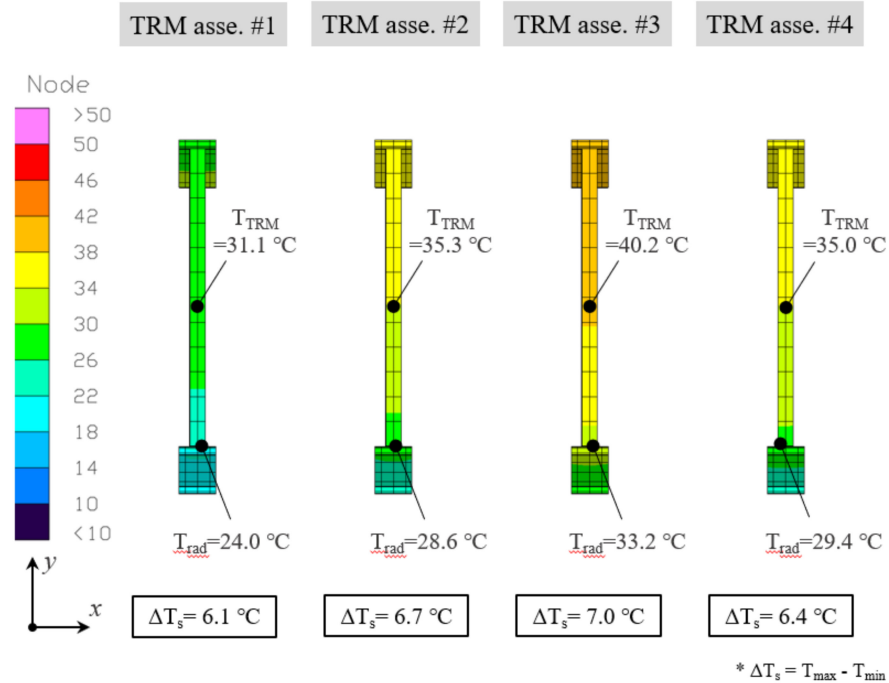


Figure 15. Spatial temperature differences (ΔT_s) of TRMs in SAR left-looking mode in hot environment (Case 1).

Table 8. Spatial temperature difference (ΔT_s) of TRM according to SAR imaging modes.

Orbital Condition	Analysis Case	Operation	Spatial Temperature Diff. (ΔT_s)			
			TRM #1	TRM #2	TRM #3	TRM #4
Hot case	Case 1	SAR imaging (Left-looking)	6.1	6.7	7.0	6.4
	Case 2	SAR imaging (Right-looking)	6.4	7.6	7.4	6.5
Cold case	Case 3	SAR imaging (Left-looking)	2.7	3.8	3.1	4.0
	Case 4	SAR imaging (Right-looking)	2.7	3.9	3.0	3.7

In this study, we also analyzed ΔT_s over the SAR radiating board and satellite primary structure because they are important in assuring the image quality of SAR antenna against the dimensional instability due to thermal distortion. Figure 16a,b, respectively, show the representative temperature contours of SAR radiating board and satellite platform structure in the left-looking SAR imaging operation in the hot environment in which the ΔT_s values are 56.6 and 13.5 °C. The antenna root-mean-square (RMS) surface error and antenna best-fit plane (ABFP) angle estimated in the previous study [22], based on those thermal analysis results, were 0.7 mm_{rms} and 0.005°, respectively. These values were sufficiently low to comply with the S-STEP SAR antenna requirements (RMS error of <1.55 mm_{rms} and ABFP angle of <0.02°).

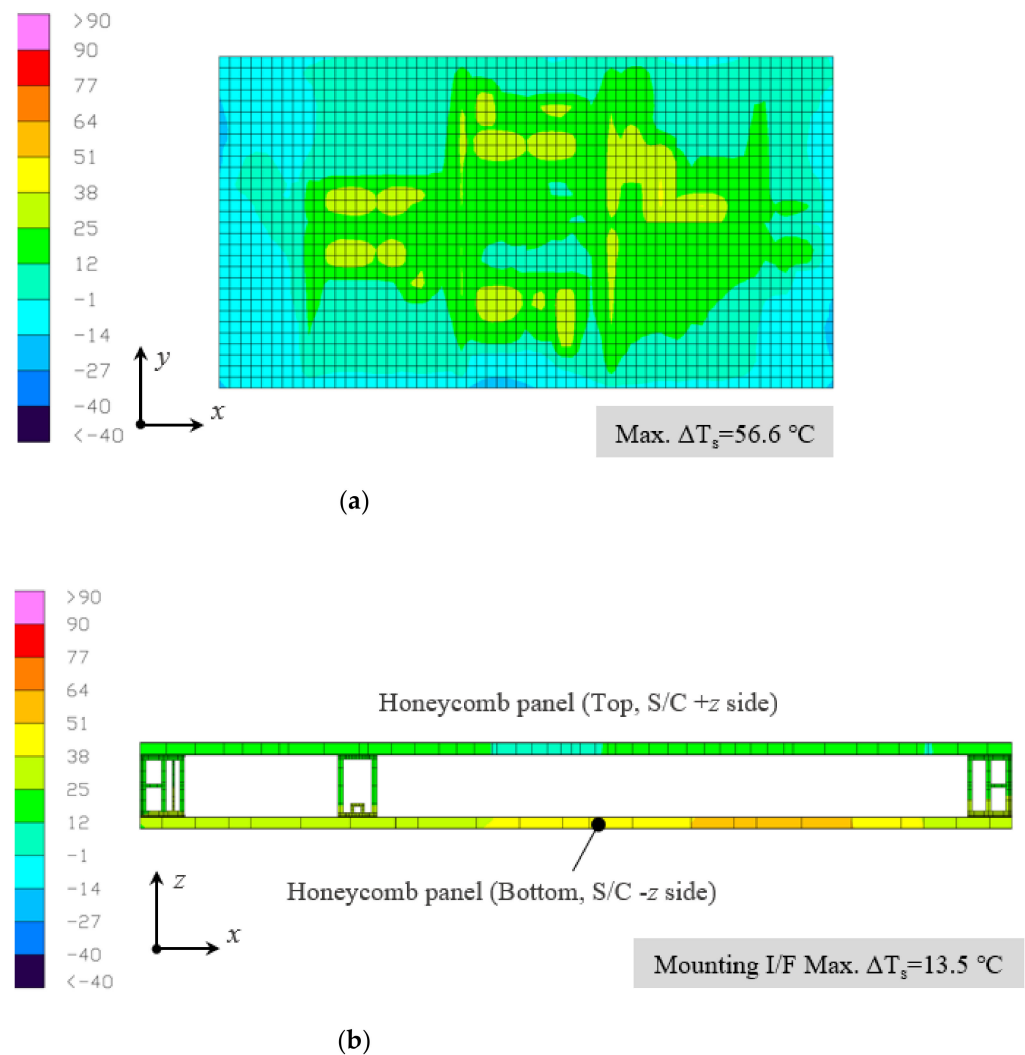


Figure 16. Spatial temperature differences (ΔT_s) of (a) SAR radiating board (b) S/C honeycomb panels in SAR left-looking mode in hot environment (Case 1).

5. Experimental Verification of Key Thermal Design

To confirm the design effectiveness of TRM radiators, a space-simulated thermal vacuum (TV) test was performed using a dummy model of TRM assembly with radiators. Figure 17 shows the configuration of the TV test set-up. The test specimen comprises a dummy TRM assembly integrated inside the test fixture. The test specimen, except for the front side of radiators, was entirely covered with MLI, and it was conductively isolated from the chamber base plate to avoid an unnecessary heat outflow from the TRM. The heat dissipation of TRM was simulated by a test heater group with 160 W power capacity attached to various locations of the dummy TRM. The heater was also applied on the rear side of each radiator to simulate the incoming environmental heat flux. In the test, the graphite sheet was not applied to the TRM structure because the test objective was to primarily verify the heat dissipation performance of the integrated radiators.

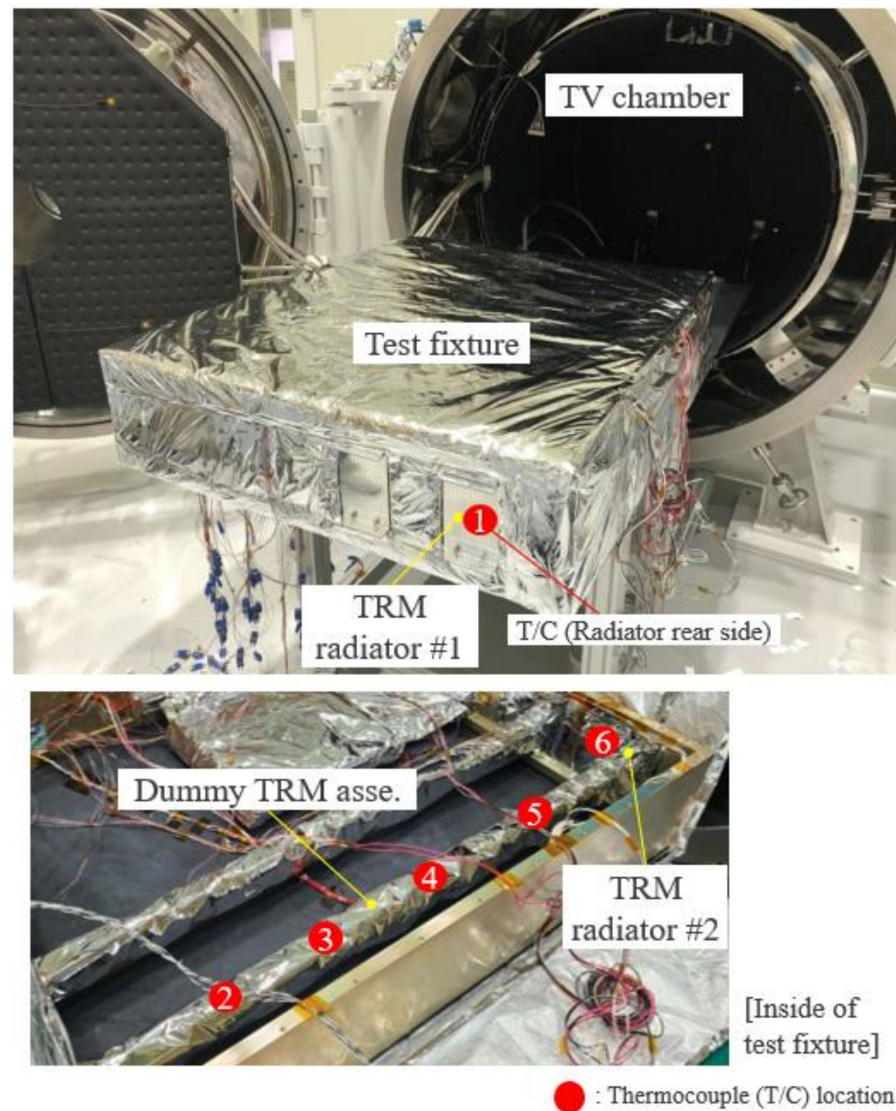


Figure 17. Thermal vacuum (TV) test set-up of dummy TRM assembly with radiators.

The specimen was exposed to the thermal environment of $-70\text{ }^{\circ}\text{C}$ controlled by a chamber shroud. The operating temperature of the radiators was maintained to $20\text{ }^{\circ}\text{C}$ by the heater control to simulate on-orbit temperature conditions. The temperature reference point was located near the center of TRM to declare thermal stabilization, as when the temperature variation is less than $2\text{ }^{\circ}\text{C}/\text{h}$. The TV test was performed under a pressure level of 10^{-5} torr. In the test, the ΔT_s between the center of the TRM and radiator was the main factor to judge the effectiveness of the proposed thermal design.

Figure 18 shows the temperature profile obtained by thermocouples when the specimen was thermally stabilized. In the thermal analysis, the orbital average heat dissipation of TRM assembly was approximately 4 W because it was operated for only 60 s during SAR imaging, although its power dissipation was 365 W . In the test, the constant heat load of 16 W was first applied to the TRM, which was a sufficiently high amount of heat load to simulate the orbital average heat dissipation. The TRM reached $25.4\text{ }^{\circ}\text{C}$, and the maximum ΔT_s between the TRM and radiator was $2.8\text{ }^{\circ}\text{C}$. Meanwhile, the thermal analysis results shown in Figure 15 indicated that the maximum ΔT_s value of TRM assemblies #1–#4 was $7.0\text{ }^{\circ}\text{C}$ when the radiator temperatures were ranging from 24.0 to $29.4\text{ }^{\circ}\text{C}$. Table 8 also shows that ΔT_s was less than $7.6\text{ }^{\circ}\text{C}$ in all cases of SAR imaging operations. The thermal conductance value between the TRM and radiator, simply estimated from the heat load and ΔT_s observed from the test, was 5.7 W/K . Subsequently, the heat load of 160 W was applied

to the TRM to observe further heat dissipation capability. The increase in TRM temperature was only less than 1 °C after 60 s, and the temperature was stabilized at 89.8 °C. The ΔT_s at the stabilized temperature was 17.4 °C. The thermal conductance value between the TRM and radiator in this condition increased to 9.2 W/K as the radiated heat energy increases at higher radiator temperature. These test results indicated that the proposed radiator design had sufficient heat dissipation capability for thermal control of TRM assembly in on-orbit SAR imaging operation conditions.

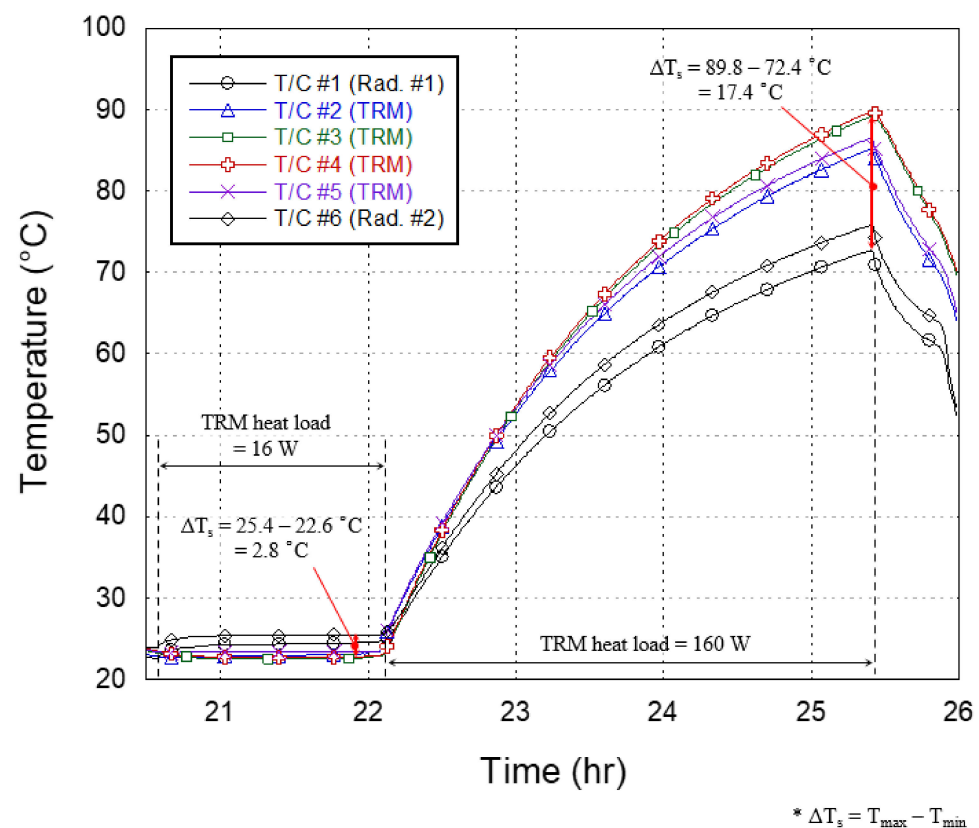


Figure 18. Temperature profiles obtained from thermocouples (T/C) of dummy TRM assembly.

6. Conclusions

In the present study, a new thermal design strategy was proposed for an 80 kg class lightweight active X-band small SAR satellite, S-STEP, for high-resolution earth observation. Considering the bus-payload integrated flat panel-type unique satellite configuration, the proposed thermal design of S-STEP mainly relied on the optimization of environmental heat flux on the satellite by passive thermal control approaches. A lightweight flexible graphite sheet with high thermal conductivity was used for heat dissipation of some high-power components via radiators. A thermal design of the key payload component of TRM assembly with dedicated radiators was proposed. To validate the effectiveness of the proposed thermal design, an on-orbit thermal analysis of S-STEP was performed in various cases of SAR-looking modes. The analysis results showed that the proposed thermal design ensured the required SAR imaging duration of 60 s regardless of left- and right-looking modes of SAR antenna while keeping all onboard components within the allowable temperature range. The spatial temperature differences in the TRM assembly and satellite primary structure of honeycomb panels were also evaluated through the analysis. The results verified that the proposed thermal design contributed to ensuring the thermal stability of the SAR payload. In the future, the effectiveness of thermal design using graphite sheets for high-power components will be experimentally verified through the TV test. In addition, the entire thermal design of S-STEP will be verified through structural-thermal model tests. The new thermal design strategy proposed in this study

would be useful and applicable to the flat panel-type small satellite for SAR observation, communication, and internet service missions.

Author Contributions: Conceptualization, H.-U.O.; methodology, H.-U.O. and B.-G.C.; validation, B.-G.C., K.-R.K.; formal analysis, B.-G.C.; investigation, B.-G.C., K.-R.K., H.-U.O.; resources, S.-C.S., H.-U.O.; data curation, B.-G.C., T.-Y.P.; writing—original draft preparation, T.-Y.P.; writing—review and editing, T.-Y.P.; visualization, T.-Y.P., B.-G.C.; supervision, H.K., S.-C.S., H.-U.O.; project administration, H.-U.O.; funding acquisition, H.K., H.-U.O. All authors have read and agreed to the published version of the manuscript.

Funding: This research was funded by the Agency for Defense Development (ADD).

Institutional Review Board Statement: Not applicable.

Informed Consent Statement: Not applicable.

Data Availability Statement: The data used to support the findings of this study are available from the corresponding author upon request.

Acknowledgments: This research was supported by the Agency for Defense Development (ADD).

Conflicts of Interest: The authors declare that they have no conflict of interest.

References

1. Morgan Stanley. The Space Economy's Next Giant Leap. 2021. Available online: <https://www.morganstanley.com/Themes/global-space-economy> (accessed on 1 September 2021).
2. Kak, A.; Akyildiz, I.F. Large-Scale Constellation Design for the Internet of Space Things/CubeSats. In Proceedings of the 2019 IEEE Globecom Workshops (GC Wkshps), Waikoloa, HI, USA, 9–13 December 2019.
3. Planet Labs Inc. Planet. Available online: <https://www.planet.com/> (accessed on 1 September 2021).
4. Starlink. Available online: <https://www.starlink.com/> (accessed on 1 September 2021).
5. Project Kuiper. Available online: <https://www.amazon.jobs/en/teams/projectkuiper> (accessed on 1 September 2021).
6. Li, J. *Satellite Remote Sensing Technologies*; Springer Nature: Cham, Switzerland, 2021.
7. Paek, S.W.; Balasubramanian, S.; Kim, S.; de Weck, O. Small-satellite synthetic aperture radar for continuous global biospheric monitoring: A review. *Remote Sens.* **2020**, *12*, 2546. [CrossRef]
8. Ignatenko, V. ICEYE Microsatellite SAR Constellation Status Update: Evaluation of first commercial imaging modes. In Proceedings of the IEEE International Geoscience and Remote Sensing Symposium (IGARSS), Waikoloa, HI, USA, 26 September–2 October 2020.
9. Capella Space. Available online: <https://www.capellaspace.com/capella-unveils-worlds-highest-resolution-commercial-sar-imagery/> (accessed on 1 September 2021).
10. Synspecive. Available online: <https://synspecive.com/satellite/satellite-strix/> (accessed on 1 September 2021).
11. i-QPS. Available online: <https://i-qps.net/> (accessed on 1 September 2017).
12. Saito, H.; Akbar, P.; Tanaka, K.; Ijichi, K.; Mita, M.; Pyne, B.; Kaneko, T.; Obata, T. Engineering-Model Results of X-band Synthetic Aperture Radar for Small Satellite and Its Application to Constellation Mission. In Proceedings of the 32nd Annual Small Satellite Conference, Logan, UT, USA, 4–9 August 2018; SSC18-VII-01, pp. 1–9.
13. Perellón, M.; Alvarez, R.; Petrini, P.; Sauer, A.; Dolce, S. Sentinel 1–spacecraft and SAR antenna thermal design, analysis, verification and flight performances. In Proceedings of the 45th International Conference on Environmental Systems (ICES), Bellevue, WA, USA, 12 July 2015.
14. Cohen, M. NovaSAR-S low cost spaceborne SAR payload design, development and deployment of a new benchmark in spaceborne radar. In Proceedings of the IEEE Radar Conference (RadarConf), Seattle, WA, USA, 8–12 May 2017.
15. Tan, C.; Yu, Z.; Sun, H.; Shi, G.; Liu, X.; Zhou, Y.; Li, G. Integrated design of X-band phased array antenna with LTCC 3D T/R module. *IEICE Electron. Express* **2020**, *17*, 1–6. [CrossRef]
16. Yang, L.; Li, Q.; Kong, L.; Gu, S.; Zhang, L. Quasi-all-passive thermal control system design and on-orbit validation of Luojia 1-01 satellite. *Sensors* **2019**, *19*, 827. [CrossRef] [PubMed]
17. Yendler, B.; Meginnis, A.; Reif, A. Thermal Management for High Power Cubesats. In Proceedings of the 34th Annual Small Satellite Conference, Logan, UT, USA, 28 July 2020; pp. 1–19.
18. Ueno, A.; Yamada, K.; Miyata, K.; Nagano, H. Proposal of Functional Thermal Control Systems for High-Power Micro-Satellite and Its Demonstration under Thermal Vacuum Condition. *J. Electron. Cool. Therm. Control* **2018**, *8*, 1–17. [CrossRef]
19. Manente, M.; Trezzolani, F.; Magarotto, M.; Fantino, E.; Selmo, A.; Bellomo, N.; Pavarin, D. REGULUS: A propulsion platform to boost small satellite missions. *Acta Astronaut.* **2019**, *157*, 241–249. [CrossRef]
20. AlShehhi, A.; AlMarar, A.; AlShehhi, Y.; AlAmeri, M. Thermal design evaluation of Loop Heat Pipe for small satellite applications using graphene Nano-Particles. In Proceedings of the 70th International Astronautical Congress (IAC), Washington, DC, USA, 21–25 October 2019.

21. Sharath, B.K.; Jotteppa, S.; Dibbi, S.; Chippalkatti, V.; Rajendran, P.; Uma Ravindra, M. Thermal Investigation of Power Supply Module (QDR-PSM) for Space Application Using Numerical and Experimental Approach. In *Advances in Small Satellite Technologies*; Springer: Singapore, 2020; pp. 493–508.
22. Kwon, S.C.; Son, J.H.; Song, S.C.; Park, J.H.; Koo, K.R.; Oh, H.U. Innovative Mechanical Design Strategy for Actualizing 80 kg-Class X-Band Active SAR Small Satellite of S-STEP. *Aerospace* **2021**, *8*, 149. [[CrossRef](#)]
23. Park, T.Y.; Oh, H.U. New PCB strain-based structural design methodology for reliable and rapid evaluation of spaceborne electronics under random vibration. *Int. J. Fatigue* **2021**, *146*, 106147. [[CrossRef](#)]
24. Kaneka Corporation. High Thermal Conductive Graphite Sheet, GraphinityTM 2021. Available online: <http://www.elecdiv.kaneka.co.jp/english/graphite/index.html> (accessed on 1 September 2021).
25. Park, D.; Miyata, K.; Nagano, H. Thermal design and validation of radiation detector for the ChubuSat-2 micro-satellite with high-thermal-conductive graphite sheets. *Acta Astronaut.* **2017**, *136*, 387–394. [[CrossRef](#)]
26. C&R Technologies. *Thermal Desktop User's Manual—A Cad Based System for Thermal Analysis and Design*; Version 6.1; C&R Technologies: Boulder, CO, USA, 2019.
27. C&R Technologies. *SINDA/FLUENT User's Manual—General Purpose Thermal/Fluid Network Analyzer*; Version 6.1; C&R Technologies: Boulder, CO, USA, 2019.
28. Adolph, M.; Hackenberg, U.; Reber, R.; Rieger, R.; Schweizer, B.; Adelseck, B.; Brugger, H.; Lorcher, M. High-precision temperature drift compensated T/R-module for satellite based SAR applications. In *Proceedings of the IEEE European Microwave Conference*, Paris, France, 4–6 October 2005.